Journal of Power Sources 196 (2011) 627–635

Contents lists available at ScienceDirect

Journal of Power Sources

journal homepage: www.elsevier.com/locate/jpowsour

Carbon-supported tetragonal MnOOH catalysts for oxygen reduction reaction in alkaline media

Wei Sun [a], Andrew Hsu [b], Rongrong Chen [a,*]

[a] Richard G. Lugar Center for Renewable Energy, Indiana University - Purdue University Indianapolis, Indianapolis, IN 46202, USA
[b] Department of Mechanical and Materials Engineering, Wright State University, Dayton, OH 45435, USA

ARTICLE INFO

Article history:
Received 26 May 2010
Received in revised form 19 July 2010
Accepted 20 July 2010
Available online 3 August 2010

Keywords:
MnOOH
Manganese oxide
Catalysts
Oxygen reduction
Carbon supports
Alkaline fuel cells

ABSTRACT

Carbon-supported MnOOH catalyst was prepared by reducing $KMnO_4$ with carbon Black Pearls 2000. TEM and XRD characterization results show that nanosized tetragonal MnOOH crystals formed in the specimen when the MnOOH content ranged from 9 wt.% to 36 wt.%. The oxygen reduction reaction (ORR) activity of the catalyst with different amounts of MnOOH content in alkaline media was investigated using a rotating disc electrode (RDE) and a rotating ring-disc electrode (RRDE). The number of electrons involved in the ORR increased from 3.2 to 3.9 with the increase of the MnOOH content from 9 wt.% to 36 wt.% in the catalyst. The kinetic current increased to 0.0184 A cm^{-2} when the MnOOH content was increased to 72 wt.%. However, both the number of electrons and the kinetic current decreased when the MnOOH content was increased from 72 wt.% to 90 wt.%. The MnOOH/C catalyst with optimized MnOOH content and suitable loading in the cathode is promising for applications in alkaline fuel cells.

1. Introduction

Recently solid alkaline fuel cells (SAFCs) based on anion exchange membranes are attracting attention as an alternative to the conventional liquid alkaline fuel cells (AFCs) and proton exchange membrane fuel cells (PEMFCs) [1–11]. Compared to AFCs and PEMFCs, SAFCs have several important advantages, including (1) facile kinetics at the cathode and the anode, (2) reduced methanol/ethanol crossover effect for direct methanol/ethanol fuel cells, (3) no electrolyte weeping, and (4) a wider range of choices of materials for current supports and bipolar plates. Furthermore, non-platinum electrocatalysts have shown significant electrocatalytic activities toward oxygen reduction reactions (ORRs) in alkaline solutions. These non-platinum electrocatalysts include carbon-supported transition metals such as Pd [12,13], Ag nano-particles [14–17], M-N_4-macrocycles [18–20], Perovskite-type oxides [21], spinel [22], as well as some transition metal oxides [23–25]. In order to successfully replace Pt electrocatalysts with the low cost materials for the cathodes of SAFCs, novel materials need to be developed and their electro-catalytic activities need to be improved.

Becase of economical and environmental considerations, manganese oxide based catalysts for the ORR in alkaline media have attracted much attention in recent years [26–31]. The catalytic activity for ORR of the manganese oxide depends on its chemical composition, structure, morphology, and preparation method. Recently, Cheng et al. [32] reported a systematic study of electrocatalytic activities of the ORRs on α-, β-, and γ-MnO_2 nanowires and had three conclusions: (1) the catalytic activities of MnO_2 depend strongly on the crystallographic structures, following an order of α- > β- > γ-MnO_2; (2) α-MnO_2 nanospheres and nanorods outperform the bulk microparticles; (3) a quasi-4 electron transfer is attained for α-MnO_2 nanostructures. These conclusions agree with what has been reported by other researchers [27,33].

Similar to manganese dioxide, MnOOH also shows catalytic activity toward ORRs [34]. MnOOH with different crystal structures and morphologies can be synthesized with several different methods. Using a hydrothermal method, a one-dimensional (1D) γ-MnOOH, such as nanorods MnOOH, was synthesized by several authors [35–38]. Mao et al. [26,39] compared the ORR activity of γ-MnOOH with that of α-Mn_2O_3, Mn_3O_4 and Mn_5O_8. The γ-MnOOH showed the highest ORR catalytic activity, which was related to the disproportionation of HO_2^-. Ohsaka et al. compared the ORR on a MnOOH-modified electrode and a superoxide dismutase (SOD) modified electrode [40,41] and found that the MnOOH is involved in sequent disproportionation of the electrochemical reduction intermediates, i.e., $O_2^{\bullet-}$ and HO_2^-. MnOOH possesses excellent catalytic activity not only for the disproportionation of the produced $O_2^{\bullet-}$ into O_2 and HO_2^-, but also for that of the produced HO_2^- into O_2 and OH^-. Because of this, a combined catalytic system with MnOOH and cobalt phthalocyanines showed almost twofold increase of the cathodic current [42]. Recently, when γ-MnOOH was coated on Pt, a

* Corresponding author. Tel.: +1 317 274 4280; fax: +1 317 274 0789.
E-mail address: rochen@iupui.edu (R. Chen).

0378-7753/$ – see front matter © 2010 Elsevier B.V. All rights reserved.
doi:10.1016/j.jpowsour.2010.07.082

significant enhancement of the electrocatalytic activity toward the ORR in alkaline media was observed [43]. In addition, MnOOH also showed excellent activities for the reduction of H_2O_2 in an alkaline media [44].

MnOOH or MnO_2 is often mixed with carbon or directly modified on glass carbon electrode for their ORR activity characterizations [32,41,45] using a rotating disk electrode. In the cathode of fuel cells, MnOOH or MnO_2 is mixed with carbon materials [46–48]. Carbon materials not only can increase the electronic conductivity of the electrode, but also has relatively good ORR catalytic activity in the alkaline media [49]. Uniform distribution of the MnO_2 into carbon is essential to high ORR catalytic activity. However, it is difficult to achieve a uniform distribution with mechanical mixing. More recently, researchers have tried to support the MnO_2 on carbon by using a chemical method instead of by simply mixing the two materials together [24,33]. The chemical method can greatly increase the uniform distribution and make it possible to achieve a good contact between manganese oxide and carbon.

Carbon-supported MnO_2 has been widely investigated for the ORR catalytic activity [24,50,51], but the study of carbon-supported MnOOH has rarely been reported, according to our best knowledge. In this work, we prepared and studied a carbon-supported MnOOH catalyst with a tetragonal crystal structure, denoted as MnOOH/C. The catalyst showed high catalytic activities toward ORR. In addition, the dependent relationships among the manganese oxide content, the morphology and the ORR activity were investigated. The optimal MnOOH/C composition for achieving the best ORR performance of oxygen electrodes was established.

2. Experimental

2.1. Catalyst synthesis

Carbon-supported MnOOH catalysts were prepared by reducing the $KMnO_4$ on the carbon material based on a method described in Refs. [52,53]. 100 mL deionized (DI) water (PURELAB) was first poured into a 500 mL distillation beaker, and 1 g of carbon (Black Pearls 2000, purchased from CABOT) was added to the beaker and mixed in an ultrasonic bath for about 30 min. Then a calculated volume of a $KMnO_4$ solution with a concentration of 2 wt.% (USP grade, purchased from Fisher Scientific) was slowly added to the beaker while continuously stirring for another 30 min. When the purple color disappeared, the beaker was put on a hot plate and refluxed at a temperature of 90 °C for 50 min. The suspension was filtered using a Buchner filter funnel, and the filtered solid was washed with DI water and dried overnight at 80 °C in an oven with a negative pressure of 25 PSI. The catalysts with different mass contents of manganese oxide were prepared by changing the weight ratio of $KMnO_4$ to carbon. For example, a catalyst with 18 wt.% MnOOH was obtained by reacting 9 mL of $KMnO_4$ with 1 g of carbon.

2.2. Physical characterization

Transmission electron microscopy (TEM) measurements of the prepared catalysts were carried out using an FEI (Hillsboro, OR) Tecnai G2 12 Bio Twin equipped with an AMT (Advanced Microscopy Techniques, Danvers, MA) CCD camera. The images were taken at 80 kV.

X-ray diffraction (XRD) patterns of the prepared catalysts were recorded with a Siemens X-ray diffractometer using Cu Kα radiation with a Ni filter. The tube current was 30 mA with a tube voltage of 40 kV. The 2θ angular regions between 10° and 90° were explored at a scan rate of 4° min^{-1}.

X-ray photoelectron spectroscopy (XPS) was recorded by a Kratos Ultra DLD imaging spectrometer (UK) using an Al Kα radiation (1486.6 eV). The binding energies were calibrated relative to C (1s) peak from carbon composition of the samples at 284.8 eV.

2.3. Electrochemical characterization using RDE and RRDE

Thin-layer working electrodes were made by depositing 20 μL of suspended catalyst ink on the surface of a glassy carbon rotating disk electrode (RDE) with a platinum ring (5.0 mm diameter as disc, Pine Instruments). The ink was taken from an aqueous suspension with 2 mg mL^{-1} of the MnOOH/C in a DI water and ethanol solvent (1:1) that was produced in an ultrasonic bath. After evaporating the water and ethanol via air-flow at room temperature for 1 h, the loading of the catalyst was 0.2 mg cm^{-2} on the working electrode.

The electrochemical experiments were carried out using an electrochemical system M2273 (PAR) to control the potential of the RDE and a rotator (Model: AFMSRCE, Pine) to control the rotating speed of the RDE. The working electrode was immersed in a 0.1 mol L^{-1} KOH (Fisher Scientific) solution saturated with either argon or oxygen (both from Praxair). A Pt wire counter electrode and a Hg/HgO reference electrode were used. All the potentials in this work, if not specified, refer to the Hg/HgO in a 0.1 mol L^{-1} KOH solution.

Hydrogen peroxide production in the O_2-saturated 0.1 mol L^{-1} KOH electrolyte was monitored with a rotating ring-disc electrode (RRDE) configuration using a polycrystalline Pt ring biased at 0.1 V vs. Hg/HgO (collection efficiency of the ring electrode $N = I_{ring}/I_{disk} = 0.21$). The potentials and the currents of the RRDE were controlled by a bipotentiostat (AFCBP1, Pine).

2.4. Oxygen electrode characterization

The oxygen electrodes, consisted of three layers: a catalyst layer, a gas diffusion layer, and a current collecting layer, were prepared based on the methods reported by Cao et al. [27]. First, the gas diffusion layer was prepared by mixing acetylene black (60 wt.%, Johnson Matthey) and PTFE emulsion (40 wt.%, Aldrich) with isopropanol (ACROS) into a paste and then rolling the paste onto a 34 × 34 mesh nickel wire cloth (Strem Chemicals). Then the catalyst layer was prepared by pasting the other side of the electrode with ink that included MnOOH/C (85 wt.%) and a PTFE emulsion (15 wt.%). The catalyst loading was 5 mg cm^{-2}. The electrode was hot pressed at a pressure of 50 kg cm^{-2} and a temperature of 200 °C for 5 min into a 0.5 mm thick sheet. Finally, the electrode sheet was sintered in the air at 250 °C for 1 h to remove organic residues.

Electrochemical measurements were carried out in a traditional three-electrode cell [27] with the oxygen electrode, described above, as the working electrode. In order to decrease the IR drop, a KOH solution of 1 mol L^{-1} instead of 0.1 mol L^{-1} was used. A graphite sheet was used as a counter electrode, and a Hg/HgO electrode was used as a reference electrode. The reference electrode was placed close to the gas electrode through a salt bridge (diameter of 1 mm). The potential of the working electrode was controlled by the electrochemical system (PAR M2273).

3. Results and discussion

3.1. Physical characterization of MnOOH/C catalysts

The MnOOH/C catalysts were prepared by reducing $KMnO_4$ with the carbon material Black Pearls 2000. The manganese oxide content was controlled by the weight ratio between the $KMnO_4$ and the carbon. Five samples with different MnOOH contents, 4.5 wt.%, 9.0 wt.%, 18 wt.%, 36 wt.%, and 72 wt.%, were prepared and characterized by TEM and XRD. Fig. 1 shows the TEM images of the catalysts. From these images, we can see that the catalyst morphology varied with the changing MnOOH content. When the MnOOH

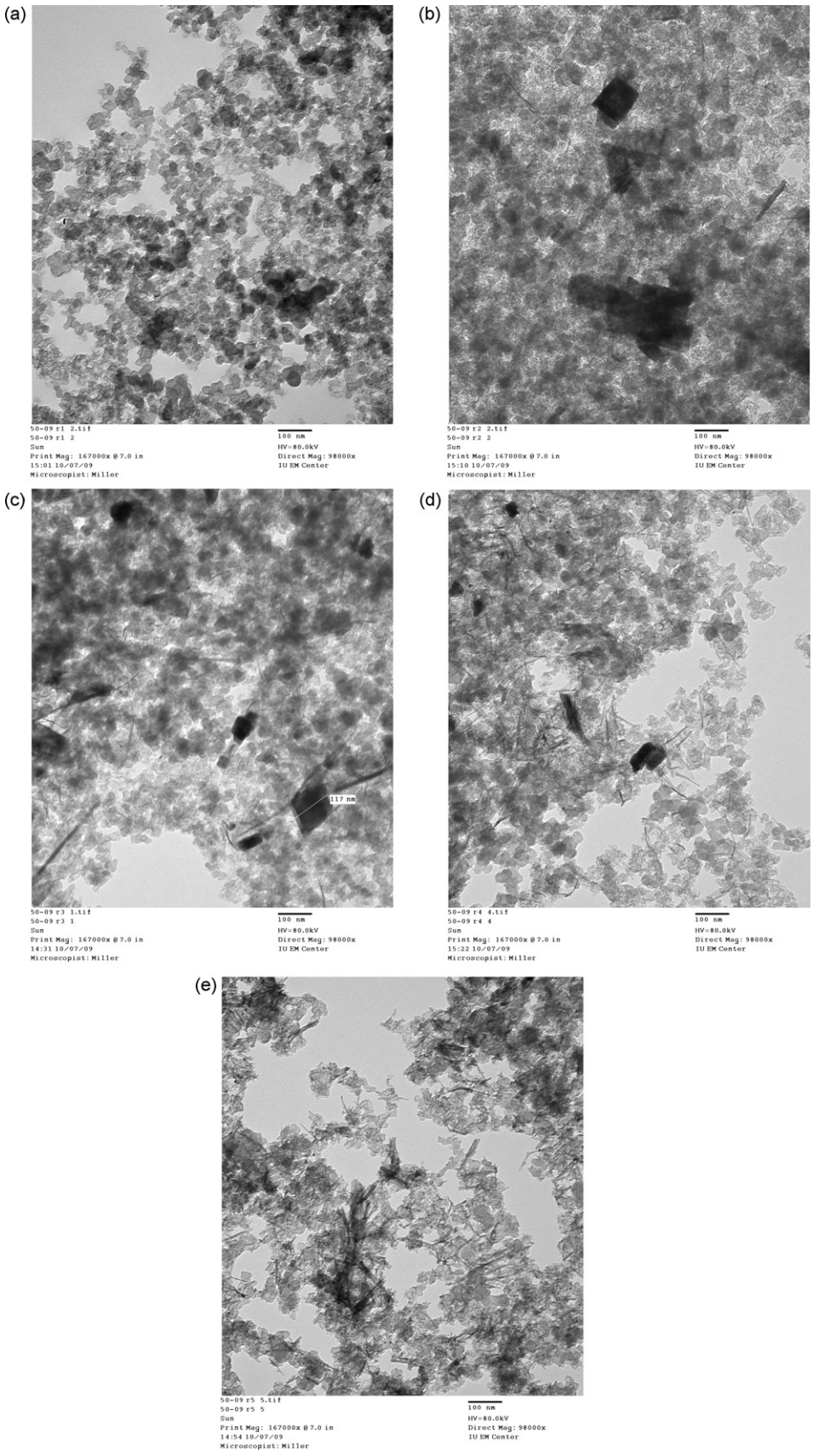

Fig. 1. TEM images of MnOOH/C with MnOOH content of (a) 4.5 wt.%, (b) 9.0 wt.%, (c) 18 wt.%, (d) 36 wt.%, and (e) 72 wt.%.

Table 1
The electrochemical kinetic parameters of carbon-supported catalysts with different MnOOH contents.

	MnOOH/C 4.5 wt.%	MnOOH/C 9 wt.%	MnOOH/C 18 wt.%	MnOOH/C 36 wt.%	MnOOH/C 72 wt.%	MnOOH/C 90 wt.%	Pt/C
Morphology	–	Tetragonal	Tetragonal	Tetragonal	Branch like	–	–
D_{mean} (nm)	–	149	145	56	–	–	–
N	3.2	3.4	3.5	3.9	3.8	3.6	4.0
i_{limt} (A cm^{-2})	0.0111	0.0118	0.0126	0.0142	0.0184	0.0145	0.0603
HO_2^- fractional yields	25.4%	24.2%	20.1%	12.8%	11.7%	9.6	2.1%

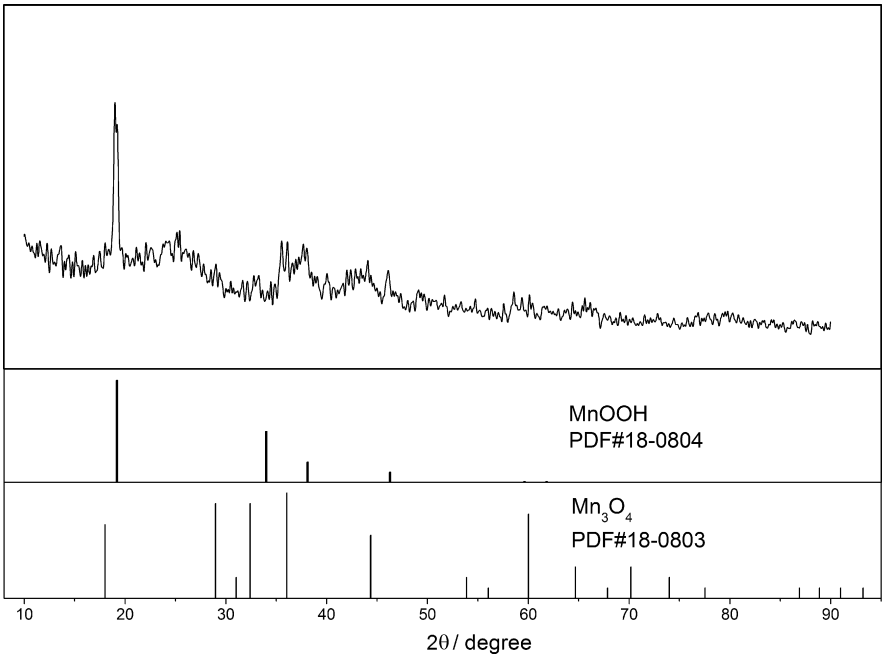

Fig. 2. X-ray diffraction (XRD) patterns for the synthesized electrocatalysts MnOOH/C 36 wt.%.

content was very low (Sample A in Fig. 1a), almost no crystal particles were observed. However, when the MnOOH content was increased to 9 wt.% (Sample B in Fig. 1b), square-shaped crystallites were observed. The morphology of the catalyst was very different compared to the reported composite with an amorphous or poor crystalline structure using similar methods [54]. When the MnOOH content was increased further, the number of crystallites was increased visibly while the particle size remained around 150 nm (Sample C in Fig. 1c). The average particle size is summarized in Table 1. It should be noted that when the MnOOH content was increased to 36 wt.% (Sample D in Fig. 1d), the square particle size became smaller, around 56 nm, and a large number of particles were uniformly distributed on the carbon support. However, when the MnOOH content was as high as 72 wt.%, the square particles disappeared unexpectedly. Instead, branch-like manganese oxide particles were observed (Sample E in Fig. 1e). As the images show, the morphology of MnOOH/C was greatly affected by the MnOOH content.

Fig. 2 shows the XRD pattern for the catalyst with a MnOOH content of 36 wt.% (Sample D). The peak at 19.2° was significantly dominant. According to the powder diffraction file (PDF#18-0804), this peak can be attributed to the tetragonal crystalline phase of β-MnOOH (feitknechite) (0 0 2) [55–57]. In this XRD pattern, other small peaks can be attributed to the Mn_3O_4 that belongs to the group of $I41/amd$, according to the powder diffraction file (PDF#18-0803). Obviously the amount of Mn_3O_4 in the catalyst was very low. The coexistence of the MnOOH and the Mn_3O_4 was also observed through other synthesis methods [58,59]. Fig. 3 shows XRD patterns for the catalysts with various MnOOH contents. The broad peaks located at 24.4° can be attributed to the graphite (0 0 2) that comes from the carbon support, Black Pearls 2000 [13]. With the increase of the MnOOH content, the peaks located at this position decreased. This phenomenon can be reasonably explained by the decrease in

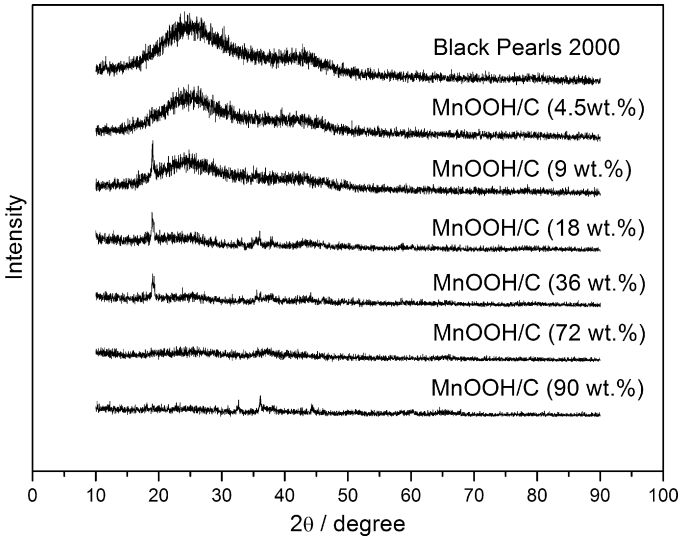

Fig. 3. X-ray diffraction (XRD) patterns for the synthesized MnOOH/C electrocatalysts. The results for Black Pearls 2000 are included for comparison.

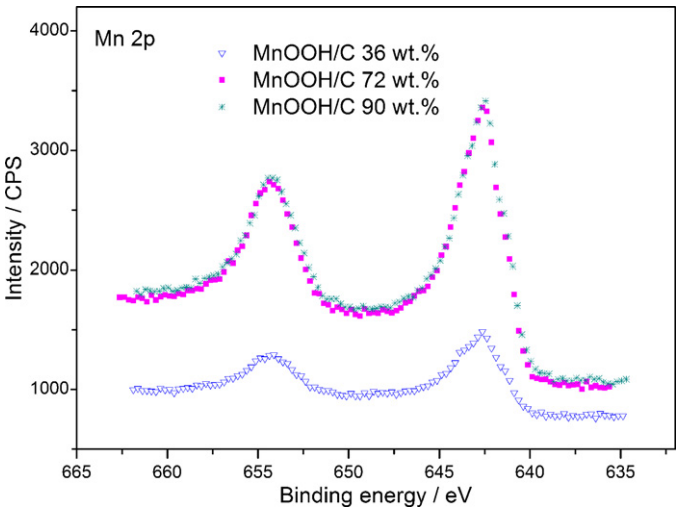

Fig. 4. Mn (2p) XPS spectra of the synthesized MnOOH/C electrocatalysts.

the relative content of carbon material. It should be emphasized that the peaks at 19.2° appeared when the MnOOH content was increased over 9 wt.% (Samples B–D). When the MnOOH content increased to as high as 72 wt.%, the peak at 19.2° became no longer detectable. The absence of the peak at 19.2° for catalysts containing MnOOH less than 9 wt.% or higher than 72 wt.% indicates that there was no crystalline phase formed in detectable amounts in the catalysts. For the MnOOH content less than 9 wt.%, the amounts of MnOOH may not be sufficient to grow measurable crystalline since the MnOOH was distributed uniformly on the Black Pearls 2000 carbon support with a large surface area. When the MnOOH content was increased to higher than 72 wt.%, the MnOOH structure may transform from the crystalline phase to an amorphous form. The TEM image (Fig. 1d) of the sample with 72 wt.% of MnOOH shows branch-like structures, which shows a very tiny peak at 19.2° in the XRD pattern. When the content of MnOOH was increased to 90 wt.%, the peak at 19.2° was no longer detectable. This result suggests the tendency that higher MnOOH content leads to a more amorphous manganese oxide. The XRD results were in good agreement with the TEM images, showing that the crystal particles were tetragonal MnOOH crystals. It should be noted that the crystal structure and morphology of the catalysts was greatly related to its composition.

XPS was conducted to evaluate the oxidation states of Mn in the synthesized catalysts. Fig. 4 shows the Mn (2p) spectrum of the catalysts with the manganese oxide content of 36 wt.%, 72 wt.%, and 90 wt.%. The observed binding energies for Mn (2p 3/2) and Mn (2p 1/2) in the catalysts were 642.4 eV and 654.2 eV. However, it is difficult to discriminate the valence state of Mn unambiguously due to some differential charging raised by the ejection of photoelectrons [60]. Fig. 5 shows the XPS results of O (1s). One can see a maximum peak near 530.2 eV for all three samples and a distinct shoulder with a pronounced tail on the high energy side of the peak. Several researchers have conducted Mn valence state investigation using O 1s spectrum [61–63]. There appears to be three spectral contributions: (1) O^{2-} or Mn–O–Mn, the oxygen bonds solely to Mn; (2) OH^{-} or Mn–O–H, the oxygen that also bonds to hydrogen; (3) H–O–H, the physisorbed and chemisorbed H_2O. They are located at 533.5 eV, 531.5 eV, and 530.2 eV, respectively. In Fig. 5, the corresponding peaks were deconvoluted for every sample. The result is in a good agreement with what was reported by Gao et al. [61], and suggests that most of the manganese oxide near the surface region of the catalysts is in the form of MnOOH.

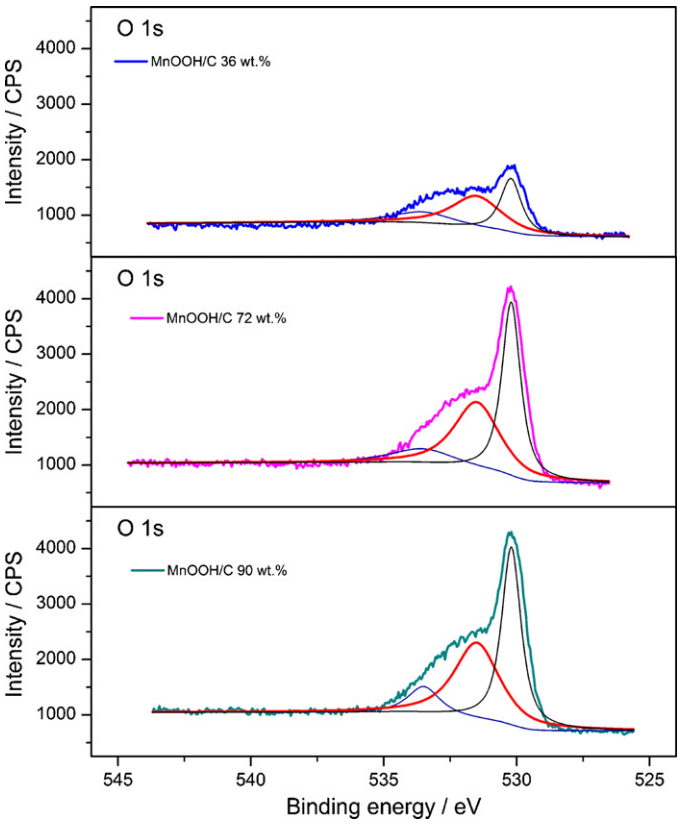

Fig. 5. O (1s) XPS spectra of the synthesized MnOOH/C electrocatalysts.

3.2. Cyclic voltammetry of the MnOOH/C catalysts

The catalytic activities of the MnOOH/C catalysts for ORR were characterized by electrochemical methods. Fig. 6 shows the cyclic voltammograms (CVs) of the catalysts in an Ar saturated 0.1 mol L^{-1} KOH solution. From the results, we can see that the oxidation–reduction of MnOOH was quasi-reversible. In the negative direction, there is a weak peak located at −0.04 V (vs. Hg/HgO). According to Lima's XANES spectra [33], MnO_2 with the IV valence was reduced to MnOOH at this potential. This sluggish peak shows that the amount of MnO_2 species in the catalyst was very low, and the Mn(IV) species may have come from the electro-oxidation of the MnOOH in the last anodic cycles. When the potential was negatively scanned to the range of −0.2 to −0.3 V, a pair of peaks with higher currents was observed. These peaks show the transition of Mn(III) to Mn(II) and may concern the intermediate product of Mn_3O_4 [33]. The small amount of Mn_3O_4 in the catalysts may also attribute to the formation of the peaks. In the positive direction, two peaks were observed. The small peak located at −0.2 V is not clear, while the highest peak at 0 V may be attributed to the formation of MnOOH from $Mn(OH)_2$. When the potential was scanned positively to 0.4 V, no obvious peaks appeared. The slight conversion of Mn(III) to Mn(IV) may have been concealed in the increasing background current. The inset graph shows that the peak currents increased with the MnOOH content in both the negative scanning and the positive scanning. This indicates that the main composition of the manganese oxide contributed to the quasi-reversible peaks and the catalyst with the manganese oxide content of 72 wt.% shows the highest peak current. The CV results show that the species with Mn(III) are dominant in the catalysts.

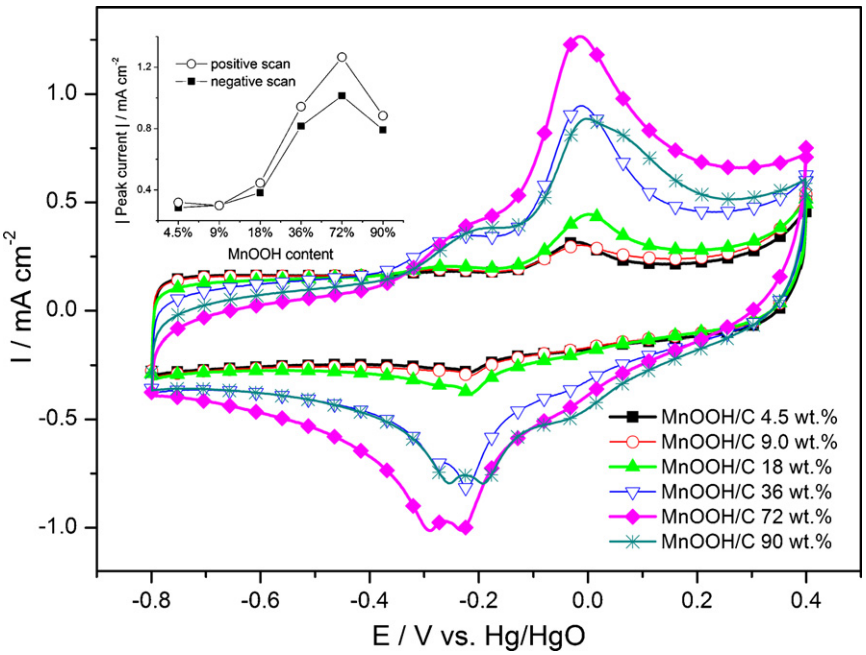

Fig. 6. Cyclic voltammograms for the synthesized MnOOH/C catalysts in a 0.1 mol L^{-1} KOH solution at room temperature, saturated with argon. The scan rate was 10 mV s^{-1}. The inset shows the peak current (peaks at −0.2 V in negative scanning and peaks at 0 V in the positive scanning) vs. MnOOH content.

3.3. Oxygen reduction activities measured by RDE and RRDE

In order to characterize the ORR activities of the synthesized MnOOH/C catalysts, a thin layer of catalyst was coated onto the RDE. Linear scanning voltammetry of the electrode was performed in 0.1 mol L^{-1} KOH solution saturated with oxygen. Fig. 7 shows the polarization curves of the catalyst with different MnOOH contents. For comparison, the polarization plot of the Pt/C catalyst with the same catalyst loading on the RDE is also shown in this figure. Obviously, the activity of the MnOOH/C catalyst was not as high as Pt/C when the onset potentials and the limiting currents were compared. The limiting current increased significantly with the increasing MnOOH content. The tendency of the limiting current to increase is in agreement with the tendency of the specific peak current increase in the CV results (Fig. 6). It is widely believed that

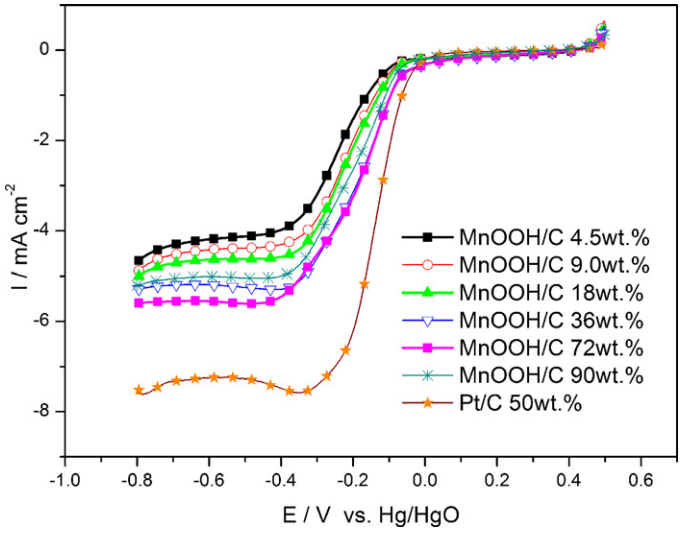

Fig. 7. The polarization curves of the catalyst with different MnOOH contents in a 0.1 mol L^{-1} KOH solution saturated with oxygen. The scan rate was 10 mV s^{-1}; the rotating speed was 2500 rpm.

the catalytic activity of MnO_2 was related to the transition reaction between Mn(IV) and Mn(III) because the potential for this transition was very close to the ORR onset potential, especially for the first 2e transition [27]. As for the MnOOH/C catalysts, the increase in the activity may be attributed to the increased proportion of the MnOOH to carbon, and the enhancement of disproportionation effect. The mass activity of the MnOOH/C at 36 wt.% can be obtained from Fig. 7 by the weight of MnOOH, 60 mA mg^{-1}, which is comparable to MnO_2 [32]. With the increase of MnOOH content, the limiting current increased initially, to a maximum value when the MnOOH content was increased to 72 wt.%. However, the limiting current decreased significantly when the MnOOH content was further increased to 90 wt.%. This may be due to a reduced electronic conductivity with high MnOOH content. Furthermore, from the voltammetric results for the ORR, we can see that the onset potential did not change much when the MnOOH content increased. Further optimization of the MnOOH content will be conducted in future fuel cell application studies.

Fig. 8 shows six sets of voltammograms of the catalysts with different MnOOH contents. With the rotating speed increase, we can see that the limiting current also increased. Fig. 9 shows the Koutecky–Levich plots for the catalysts obtained from the limiting current (at −0.6 V vs. Hg/HgO) in Fig. 8. From the slopes and intercepts, the number of electrons involved in the ORR and the kinetic limiting current can be obtained. The results are shown in Table 1. We can see that with the MnOOH content increase, the number of electrons increased from 3.2 to the highest value, 3.9, which is very close to the number for the ORR on Pt/C catalysts. The quasi-4e ORR pathway is in agreement with other types of carbon-supported manganese oxide [50,64,65]. When the MnOOH content was increased to 72 wt.% and even to 90 wt.%, the number of electrons decreased quickly. In addition, the kinetic current increases with the MnOOH content increasing. The highest limiting current of 0.0184 A cm^{-2} was obtained when the MnOOH content was increased to as high as 72 wt.%. This is in agreement with the result of Fig. 7. When the MnOOH content was increased to 90 wt.%, the kinetic current also decreased. The existence of optimized MnOOH content was in agreement with reported results [52]. For the catalysts with high MnOOH contents, the amorphous

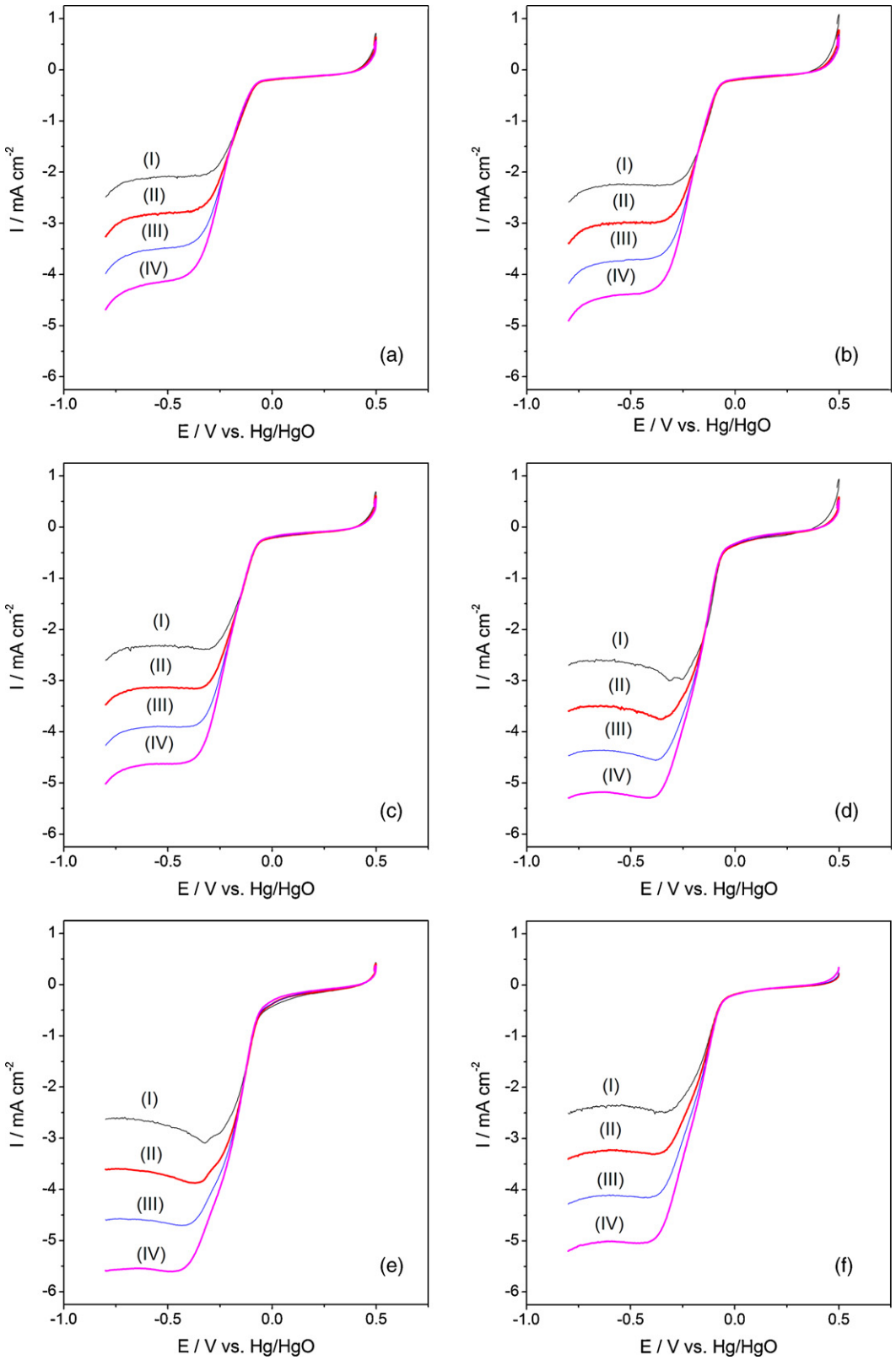

Fig. 8. Hydrodynamic voltammograms for O_2 reduction on MnOOH/C with different MnOOH contents: (a) 4.5 wt.%, (b) 9.0 wt.%, (c) 18 wt.%, (d) 36 wt.%, (e) 72 wt.%, and (f) 90 wt.% in a 0.1 mol L^{-1} KOH solution at room temperature, saturated with oxygen. The rotating speed: I: 400 rpm; II: 900 rpm; III: 1600 rpm; IV: 2500 rpm.

and poorly crystalline MnOOH may attribute to the decrease in the ORR activity [28].

It is important to discuss how the MnOOH content affected the intermediate product of HO_2^-. The experiments were carried out using a RRDE. The ring electrode potential was set at 100 mV (vs. Hg/HgO) because this potential was high enough to oxidize the hydrogen peroxide ions, but it was not too high to alleviate the ring electrode sensitivity. The ring currents corresponding to the disc currents are shown in Fig. 10. For comparison, the results of carbon and Pt/C catalysts are also included in this figure. With the

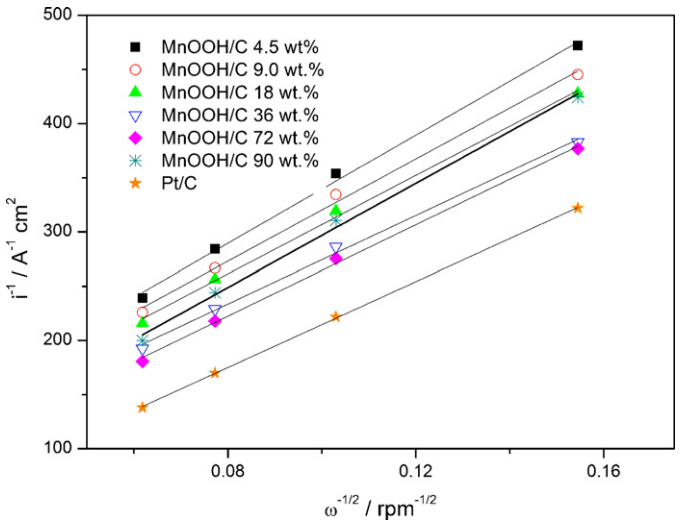

Fig. 9. Koutecky–Levich plots for the ORR on MnOOH/C with different MnOOH contents: (a) 4.5 wt.%, (b) 9.0 wt.%, (c)18 wt.%, (d) 36 wt.%, (e)72 wt.%, and (f) 90 wt.% in a 0.1 mol L^{-1} KOH saturated with oxygen.

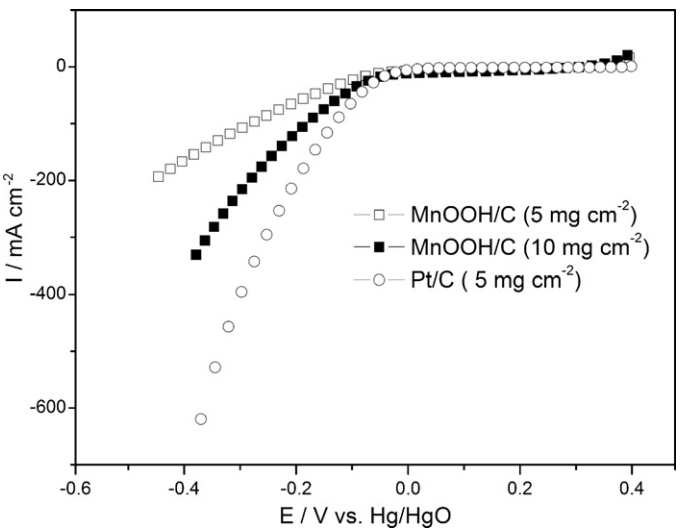

Fig. 11. The polarization curves of the electrodes with a MnOOH/C catalyst (36 wt.%) loading of 5 mg cm^{-2} and 10 mg cm^{-2}. The result of Pt/C was also shown as a bench mark. Aqueous solution: 1 mol L^{-1} KOH; scan rate: 10 mV s^{-1}.

increase of the MnOOH content, the ring current decreased significantly, showing that the intermediate product of H_2O_2 was greatly decreased. The hydrogen peroxide fractional yield can be calculated as described in the literature [13]. The results are listed in Table 1, which confirms the ORR activities of the MnOOH/C catalysts with the MnOOH content increasing. It should be noted that when the MnOOH content of the catalyst increased higher than 36 wt.%, HO_2^- yield was greatly decreased from more than 20% to about 10%.

3.4. Oxygen reduction at oxygen electrode

According to the RDE results, the MnOOH/C catalyst shows a promising ORR activity. However the catalyst needs to be characterized in an oxygen electrode to evaluate its performance in a fuel cell test environment. The MnOOH/C catalyst with a MnOOH content of 36 wt.% was employed as an active composition in the catalytic layer of an oxygen electrode, and the electrode was tested in a home-made cell, as described in Section 2. Using this method, the oxygen was diffused through a diffusion layer instead of through an aqueous solution, so the oxygen transferring resistance was greatly alleviated, and thus, the current density of the electrode was enhanced. Fig. 11 shows the polarization results of the oxygen electrodes after the IR drop correction. The original data was obtained by scanning the potential negatively while the diffusion layer of the electrodes was simultaneously fed with oxygen. In this experiment, the oxygen electrodes with the catalyst loading of 5 mg cm^{-2} and 10 mg cm^{-2} were characterized, respectively. As a bench mark, the electrode with the Pt/C catalyst was also tested under the same conditions. From the results, we can see that the current density on the oxygen electrode with the MnOOH/C catalyst was still lower than that of the Pt/C catalyst, so the activity of the MnOOH/C catalyst was still inferior to that of the Pt/C catalyst. However, with the increase of the MnOOH catalyst loading on the catalytic layer, the polarization curve of the catalyst became closer to that of the Pt/C catalyst. It apparently indicated that an increase of the loading of the MnOOH/C catalyst greatly enhanced the electrocatalytic properties. So by properly tuning the cathode, the MnOOH/C material shows promising application for the alkaline fuel cells.

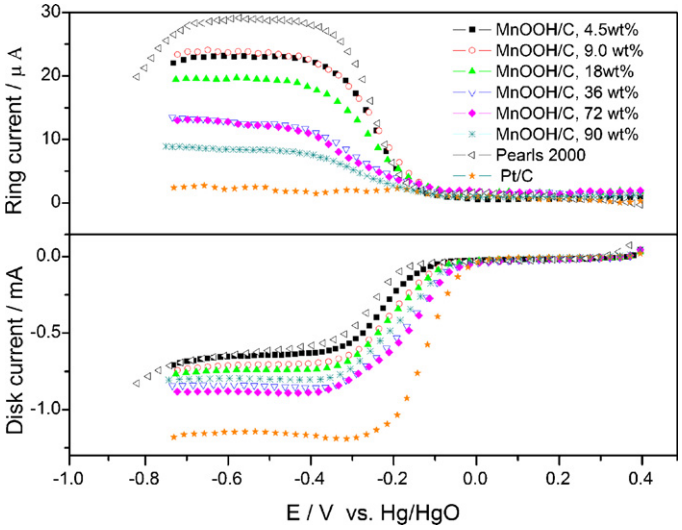

Fig. 10. The RRDE experimental results of the MnOOH/C catalysts with different MnOOH contents. KOH solution: 0.1 mol L^{-1}, saturated with oxygen; scan rate: 10 mV s^{-1}; rotating speed: 1600 rpm.

4. Conclusions

A carbon-supported tetragonal MnOOH catalyst was obtained by reducing $KMnO_4$ with carbon materials and having the MnOOH content in a range of 9–36 wt.%. The nanoparticle size of the crystal on the carbon decreased to about 50 nm when the MnOOH content increased from 9 wt.% to 36 wt.%. The morphology of the catalyst was greatly affected by the MnOOH content. Higher MnOOH content tends to form higher contents of amorphous structures. When the MnOOH content was increased from 9 wt.% to 36 wt.%, the electron number involved in the ORR increased from 3.4 to 3.9. The catalytic activity for the ORR increased as the MnOOH content increases. When the MnOOH content increased to 72 wt.%, the kinetic current was increased to 0.0184 A cm^{-2}. Upon further increase of the content to 90 wt.%, both the electron number and the kinetic current decreased. The oxygen electrodes with higher catalyst loading showed higher ORR activities. Thus, the carbon-supported nanosized MnOOH catalyst shows potential for applications in alkaline fuel cells.

Acknowledgment

This work was supported by the U.S. Army Research Lab (Grant No. W911NF-07-2-0036).

References

[1] K. Scott, E. Yu, G. Vlachogiannopoulos, M. Shivare, N. Duteanu, J. Power Sources 175 (2008) 452–457.
[2] J.R. Varcoe, R.C.T. Slade, Electrochem. Commun. 8 (2006) 839–843.
[3] F. Bidault, D.J.L. Brett, P.H. Middleton, N.P. Brandon, J. Power Sources 187 (2009) 39–48.
[4] L. Li, Y.X. Wang, J. Membr. Sci. 262 (2005) 1–4.
[5] X.-B. Zhang, J.-M. Yan, S. Han, H. Shioyama, K. Yasuda, N. Kuriyama, Q. Xu, J. Power Sources 182 (2008) 515–519.
[6] E.H. Yu, K. Scott, J. Power Sources 137 (2004) 248–256.
[7] Y. Xiong, Q.L. Liu, A.M. Zhu, S.M. Huang, Q.H. Zeng, J. Power Sources 186 (2009) 328–333.
[8] S. Gu, R. Cai, T. Luo, Z. Chen, M. Sun, Y. Liu, G. He, Y. Yan, Angew. Chem. 121 (2009) 6481.
[9] Y. Wan, B. Peppley, K.A.M. Creber, V.T. Bui, E. Halliop, J. Power Sources 185 (2008) 183–187.
[10] C. Tamain, S.A. Poynton, R.C.T. Slade, B. Carroll, J.R. Varcoe, J. Phys. Chem. C 111 (2007) 18423–18430.
[11] Y.W. Guigui Wang, D. Chu, R. Chen, D. Xie, J. Membr. Sci. 332 (2009) 63–68.
[12] L. Jiang, A. Hsu, D. Chu, R. Chen, J. Electrochem. Soc. 156 (2009) B643–B649.
[13] L. Jiang, A. Hsu, D. Chu, R. Chen, J. Electrochem. Soc. 156 (2009) B370–B376.
[14] J. Guo, A. Hsu, D. Chu, R. Chen, J. Phys. Chem. C 114 (2010) 4324–4330.
[15] J.R. Varcoe, R.C.T. Slade, G.L. Wright, Y.L. Chen, J. Phys. Chem. B 110 (2006) 21041–21049.
[16] K. Ni, L. Chen, G. Lu, Electrochem. Commun. 10 (2008) 1027–1030.
[17] M.A. Kostowskyj, R.J. Gilliam, D.W. Kirk, S.J. Thorpe, Int. J. Hydrogen Energy 33 (2008) 5773–5778.
[18] R. Chen, H. Li, D. Chu, G. Wang, J. Phys. Chem. C 113 (2009) 20689–20697.
[19] F. Harnisch, N.A. Savastenko, Z. Feng, H. Steffen, V. Bruser, U. Schroder, J. Power Sources 193 (2009) 86–92.
[20] C. Song, L. Zhang, J. Zhang, D.P. Wilkinson, R. Baker, Fuel Cells 7 (2007) 9–15.
[21] K. Miyazaki, N. Sugimura, K. Matsuoka, Y. Iriyama, T. Abe, M. Matsuoka, Z. Ogumi, J. Power Sources 178 (2008) 683–686.
[22] E. Rios, H. Reyes, J. Ortiz, J.L. Gautier, Electrochim. Acta 50 (2005) 2705–2711.
[23] F.H.B. Lima, M.L. Calegaro, E.A. Ticianelli, J. Electroanal. Chem. 590 (2006) 152–160.
[24] K.P. Gong, P. Yu, L. Su, S.X. Xiong, L.Q. Mao, J. Phys. Chem. C 111 (2007) 1882–1887.
[25] M.L. Calegaro, F.H.B. Lima, E.A. Ticianelli, J. Power Sources 158 (2006) 735–739.
[26] L.Q. Mao, D. Zhang, T. Sotomura, K. Nakatsu, N. Koshiba, T. Ohsaka, Electrochim. Acta 48 (2003) 1015–1021.
[27] Y.L. Cao, H.X. Yang, X.P. Ai, L.F. Xiao, J. Electroanal. Chem. 557 (2003) 127–134.
[28] J. Yang, J.J. Xu, Electrochem. Commun. 5 (2003) 306–311.
[29] A. Verma, A.K. Jha, S. Basu, J. Power Sources 141 (2005) 30–34.
[30] F.P. Hu, X.G. Zhang, F. Xiao, J.L. Zhang, Carbon 43 (2005) 2931–2936.
[31] G.-Q. Zhang, X.-G. Zhang, Y.-G. Wang, Carbon 42 (2004) 3097–3102.
[32] F. Cheng, Y. Su, J. Liang, Z. Tao, J. Chen, Chem. Mater. 22 (2009) 898–905.
[33] F.H.B. Lima, M.L. Calegaro, E.A. Ticianelli, Electrochim. Acta 52 (2007) 3732–3738.
[34] K. Matsuki, H. Kamada, Electrochim. Acta 31 (1986) 13–18.
[35] Y.G. Zhang, Y. Liu, F. Guo, Y.H. Hu, X.Z. Liu, Y.T. Qian, Solid State Commun. 134 (2005) 523–527.
[36] R.Z. Yang, Z.X. Wang, L. Dai, L.Q. Chen, Mater. Chem. Phys. 93 (2005) 149–153.
[37] J. Wu, H. Zhang, X. Ma, J. Li, F. Sun, N. Du, D. Yang, Mater. Lett. 60 (2006) 3895–3898.
[38] P.K. Sharma, M.S. Whittingham, Mater. Lett. 48 (2001) 319–323.
[39] M. Lanqun, T. Sotomura, K. Nakatsu, N. Koshiba, Z. Dun, T. Ohsaka, J. Electrochem. Soc. 149 (2002) A504–507.
[40] L.Q. Mao, K. Arihara, T. Sotomura, T. Ohsaka, Chem. Commun. (2003) 2818–2819.
[41] T. Ohsaka, L. Mao, K. Arihara, T. Sotomura, Electrochem. Commun. 6 (2004) 273–277.
[42] K. Arihara, L. Mao, P.A. Liddell, E. Marino-Ochoa, A.L. Moore, T. Imase, D. Zhang, T. Sotomura, T. Ohsaka, J. Electrochem. Soc. 151 (2004) A2047–A2052.
[43] M.S. El-Deab, T. Ohsaka, J. Electrochem. Soc. 155 (2008) D14–D21.
[44] W. Chen, N. Wang, L. Liu, Y.R. Cui, X. Cao, Q.J. Chen, L. Guo, Nanotechnology 20 (2009).
[45] F.Y. Cheng, J. Shen, W.Q. Ji, Z.L. Tao, J. Chen, ACS Appl. Mater. Interfaces 1 (2009) 460–466.
[46] C.-C. Yang, S.-J. Chiu, W.-C. Chien, J. Power Sources 162 (2006) 21–29.
[47] Y.-G. Wang, Y.-Y. Xia, Electrochem. Commun. 8 (2006) 1775–1778.
[48] D. Qu, J. Power Sources 156 (2006) 692–699.
[49] I. Kruusenberg, M. Marandi, V. Sammelselg, K. Tammeveski, Electrochem. Solid State Lett. 12 (2009) F31–F34.
[50] I. Roche, K. Scott, J. Electroanal. Chem. 638 (2010) 280–286.
[51] B. Klapste, J. Vondrak, J. Velicka, Electrochim. Acta 47 (2002) 2365–2369.
[52] M.O. Danilov, A.V. Melezhyk, J. Power Sources 163 (2006) 376–381.
[53] N. Ominde, N. Bartlett, X.-Q. Yang, D. Qu, J. Power Sources 185 (2008) 747–753.
[54] P. Bezdicka, T. Grygar, B. Klapste, J. Vondrak, Electrochim. Acta 45 (1999) 913–920.
[55] X.H. Feng, W.F. Tan, F. Liu, Q.Y. Huang, X.W. Liu, Sci. China Ser. D: Earth Sci. 48 (2005) 1438–1451.
[56] J.A. Luo, Q.H. Zhang, S.L. Suib, Inorg. Chem. 39 (2000) 741–747.
[57] F. Zhou, X.M. Zhao, C.G. Yuan, H. Xu, J. Mater. Sci. 42 (2007) 9978–9982.
[58] C.C. Hu, Y.T. Wu, K.H. Chang, Chem. Mater. 20 (2008) 2890–2894.
[59] S. Shanmugam, A. Gedanken, J. Phys. Chem. C 112 (2008) 15752–15758.
[60] M. Chigane, M. Ishikawa, J. Electrochem. Soc. 147 (2000) 2246–2251.
[61] T. Gao, F. Krumeich, R. Nesper, H. Fjellvag, P. Norby, Inorg. Chem. 48 (2009) 6242–6250.
[62] H.W. Nesbitt, D. Banerjee, Am. Mineral. 83 (1998) 305–315.
[63] M. Ramstedt, A.V. Shchukarev, S. Sjoberg, Surf. Interface Anal. 34 (2002) 632–636.
[64] N. Ohno, Y. Akeboshi, M. Saito, J. Kuwano, H. Shiroishi, T. Okumura, Y. Uchimoto, Top. Catal. 52 (2009) 903–911.
[65] Y. Su, J. Liang, Z. Tao, J. Chen, Chem. Mater. (2009).